Int. J. Mol. Sci. **2014**, *15*, 5032-5044; doi:10.3390/ijms15035032

OPEN ACCESS
International Journal of
Molecular Sciences
ISSN 1422-0067
www.mdpi.com/journal/ijms

Article

Atmospheric Oxidation Mechanism and Kinetic Studies for OH and NO_3 Radical-Initiated Reaction of Methyl Methacrylate

Rui Gao [1], Ledong Zhu [2], Qingzhu Zhang [1,*] and Wenxing Wang [1]

[1] Environment Research Institute, Shandong University, Ji'nan 250100, China;
E-Mails: sdgaorui@hotmail.com (R.G.); wxwang@sdu.edu.cn (W.W.)
[2] School of Chemistry and Chemical Engineering, Shandong University, Ji'nan 250100, China;
E-Mail: georgerui@sohu.com

* Author to whom correspondence should be addressed; E-Mail: zqz@sdu.edu.cn;
Tel.: +86-531-8836-4435; Fax: +86-531-8836-1990.

Received: 18 December 2013; in revised form: 12 February 2014 / Accepted: 5 March 2014 / Published: 20 March 2014

Abstract: The mechanism for OH and NO_3 radical-initiated oxidation reactions of methyl methacrylate (MMA) was investigated by using density functional theory (DFT) molecular orbital theory. Geometrical parameters of the reactants, intermediates, transition states, and products were fully optimized at the B3LYP/6-31G(d,p) level. Detailed oxidation pathways were presented and discussed. The rate constants were deduced by the canonical variational transition-state (CVT) theory with the small-curvature tunneling (SCT) correction and the multichannel Rice-Ramspergere-Kassele-Marcus (RRKM) theory, based on the potential energy surface profiles over the general atmospheric temperature range of 180–370 K. The calculated results were in reasonable agreement with experimental measurement.

Keywords: atmospheric oxidation; methyl methacrylate; rate constants; reaction mechanism

1. Introduction

Methyl methacrylate (MMA, $CH_3COOCH_2CH_3$) is widely used in manufacture of resins and plastics [1–3]. Currently, over 2.04×10^9 kg of MMA has been produced by industrial processes [4]. Since the increasing use of MMA, the emission into the atmosphere may greatly rise. The high vapor pressure (3.9×10^3 Pa at 293 K) indicates that MMA exists mainly in the gas phase under the general atmospheric conditions [5,6]. Neurological symptoms have been reported in humans following acute

exposure to methyl methacrylate [7,8]. Fetal abnormalities have been reported in animals exposed to methyl methacrylate by injection and inhalation [9]. Once released into the atmosphere, the unsaturated MMA may be oxidized by OH radicals during daytime, nitrate radicals (NO_3), and ozone molecules during the nighttime [10,11]. The most important oxidation degradation of MMA is initiated by reaction with OH radicals in the atmosphere. However, as the formation of OH mainly takes place in daytime, OH concentration rapidly decreases after sunset. As a consequence, reactions with OH radicals only occur during the day. NO_3 radical undergoes rapid photolysis upon absorption of radiation. During daytime, concentration of NO_3 radicals is very low. Therefore, daytime NO_3 chemistry is expected to be unimportant for the MMA. However, NO_3 has been identified and measured in the nighttime atmosphere, especially in some seriously polluted regions. The reactions with NO_3 will dominate the loss pathway of MMA during nighttime. Moreover, in certain locations during certain times of the year, reactions with Cl atoms may also be important. These atmospheric oxidation reactions may contribute to the formation of the secondary photooxidants and aerosols in the troposphere.

The large emission, high volatility, and toxicity of MMA make it a potential important source of environmental concern in the atmosphere. The previous studies on the atmospheric reaction of MMA mainly focus on obtaining kinetic parameters. Low pressure rate constant for the reaction of MMA with OH radicals has been determined using the discharge flow-laser induced fluorescence (DF/LIF) technique at the room temperature [12]. The rate constants for the reactions of MMA with OH radicals and Cl atoms were carried out using the relative rate methods at the ambient temperature and pressure conditions [13], giving $k_{OH} = (4.15 \pm 0.32) \times 10^{-11}$ cm^3 molecule^{-1} s^{-1}, and $k_{Cl} = (2.82 \pm 0.93) \times 10^{-10}$ cm^3 molecule^{-1} s^{-1}. Arrhenius formula over the temperature range of 253−374 K was derived as $k(T)$(MMA + OH) = $(2.5 \pm 0.8 \times 10^{-12}) \exp((825 \pm 55)/T)$ cm^3 molecule^{-1} s^{-1}. The rate constants for the gas-phase reactions of a series of acrylate methyl (including MMA) with O_3 were determined using smog chamber techniques [14] at 1.01×10^4 Pa and 294 ± 2 K. The rate constant of MMA was obtained as $k_{O3} = (6.7 \pm 0.9) \times 10^{-18}$ cm^3 molecule^{-1} s^{-1}. Recently, the reactions of MMA with OH radicals in the presence of NOx were studied in environmental chamber [15], revealing that the primary products are methyl pyruvate (92% ± 16%) and methanal (87% ± 12%). However, due to the scarcity of efficient detection schemes for radical intermediate species and commercially available standards, the atmospheric reaction mechanism of MMA is still unclear. In this work, quantum chemical and direct kinetic calculations were performed to elucidate the reaction mechanism of the OH and NO_3 radical-initiated atmospheric oxidation of MMA.

2. Results and Discussion

To confirm the reliability of calculated results, the geometries and vibrational frequencies of $CH_3COOCH_2CH_3$, CH_3CHO, and $CH_3CH{=}CH_2$ were calculated at the B3LYP/6-31G(d,p) level. The results are in reasonable accordance with the corresponding experimental values and the discrepancy remains within 1% for geometrical parameters and 4% for vibrational frequencies [16,17].

2.1. Reaction Mechanism

The reactions of MMA with OH and NO_3 radicals involve two kinds of pathways: H abstraction from MMA and addition of OH or NO_3 radical to the C=C bond. The reaction schemes embedded with

the potential barriers and reaction enthalpies are depicted in Figures 1 and 2. For convenience of description, the C and H atoms in MMA are labeled, as depicted in Figures 1–6.

Figure 1. OH radical-initiated reaction schemes embedded with the potential barriers Δ*E* (in kcal/mol) and reaction heats Δ*H* (in kcal/mol, 0 K).

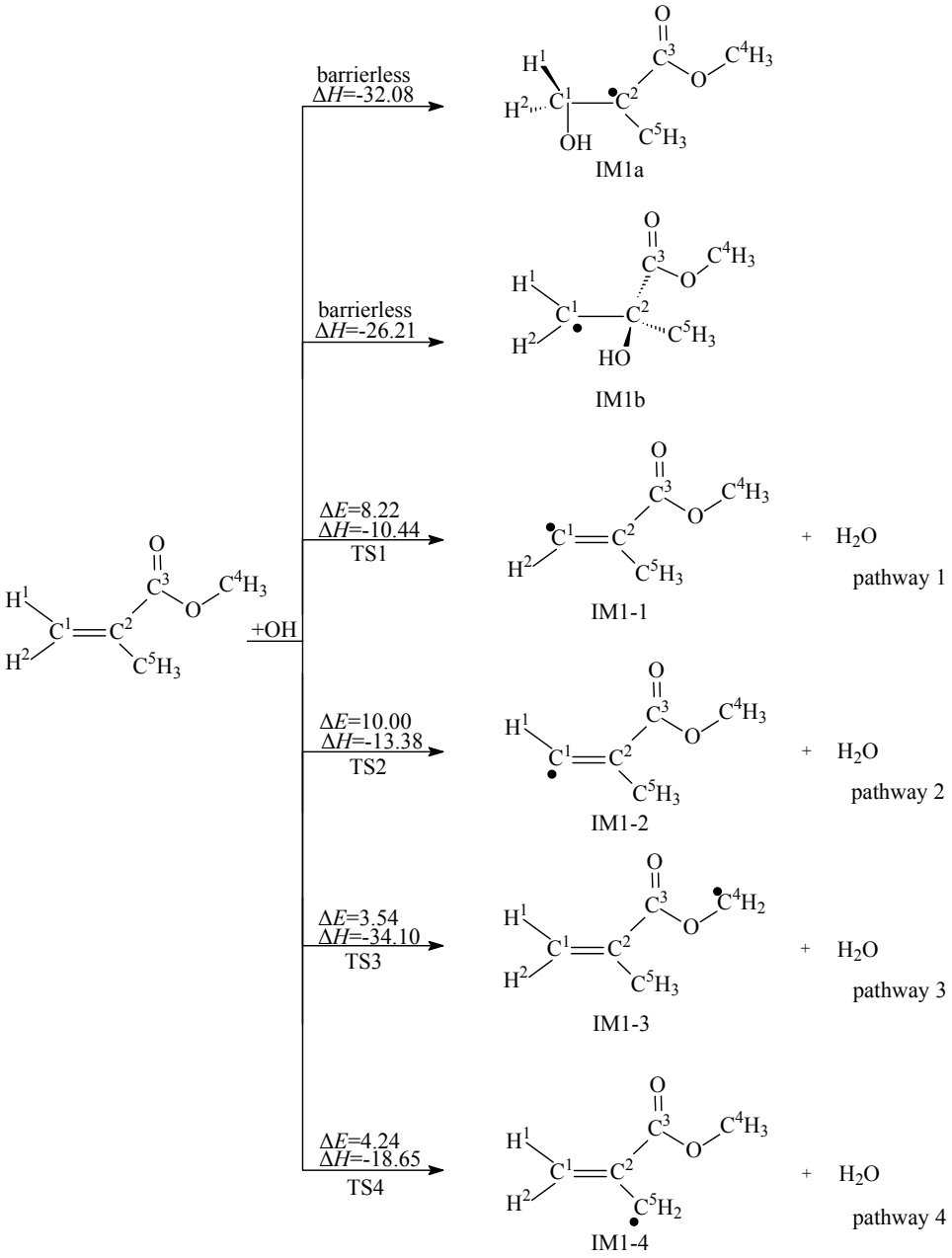

2.1.1. H Abstraction by OH and NO_3 Radicals

As shown in Figures 1 and 2, there are eight H atoms in the MMA molecule. Since the C^2–C^5 and O–C^4 bonds are rotatable, three H atoms bonded to C^4 are equivalent, and three H atoms bonded C^5 are equivalent. So, there are four kinds of H atoms in the MMA molecule, indicating that four possible pathways can be identified: H abstraction from the C^1–H^1, C^1–H^2, C^4–H, and C^5–H bonds. The products of H abstraction by OH or NO_3 radicals are IM1-1, IM1-2, IM1-3, and IM1-4. Eight transition states were located (TS1, TS2, TS3, and TS4 for H abstraction by OH radicals and TS1',

TS2', TS3', and TS4' for H abstraction by NO_3 radicals), and each one was identified with only one imaginary frequency. The reaction schemes embedded with the potential barriers and reaction heats are depicted in Figures 1 and 2. All the H abstraction processes are exothermic. The potential barriers of pathways 3 and 4 are lower than that of pathways 1 and 2. In addition, pathways 3 and 4 are more exothermic than pathways 1 and 2. Thus, the thermodynamically favored H abstraction pathways are pathways 3 and 4. The resulting IM1-3 and IM1-4 are the main H abstraction products. Similarly, pathways 7 and 8 are thermodynamically favored H abstraction pathways for the reaction of MMA with NO_3 radicals. Two same products, IM1-3 and IM1-4, can be yielded from pathways 7 and 8. Therefore, IM1-3 and IM1-4 are important intermediates produced in the oxidation process of MMA initiated by OH and NO_3 radicals.

Figure 2. NO_3 radical-initiated reaction schemes embedded with the potential barriers ΔE (in kcal/mol) and reaction heats ΔH (in kcal/mol, 0 K).

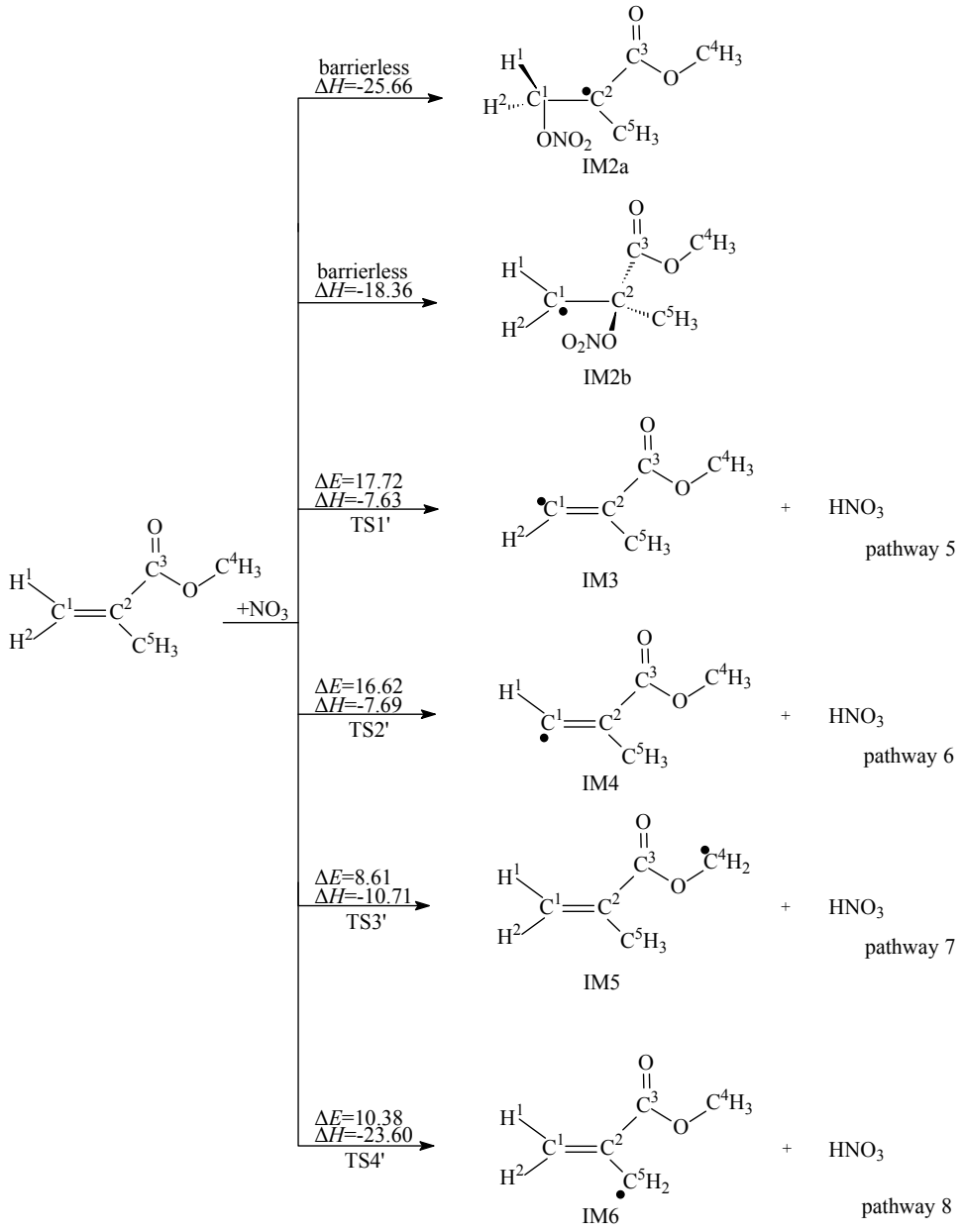

IM1-3 and IM1-4 are activated radicals and can further react with the ubiquitous oxygen molecules in the atmosphere to form two organic peroxy radicals, IM1-5 and IM1-8. To evaluate the nature of the entrance channel for the formation of the organic peroxy radicals of IM1-5 and IM1-8, we examined the potential along the reaction coordinate, especially to determine whether there is a well-defined transition state or if the process proceeds via a loose transition state without a barrier, depicted in Figure 3. The profiles of the potential energy surface were scanned by varying the newly formed C^4–O or C^5–O bond. We found no energy exceeding the C^4–O or C^5–O bond dissociation threshold along the reaction coordinate. This shows that the reactions of IM1-3 and IM1-4 with O_2 proceed via a barrierless association. The processes are strongly exothermic by 32.19 and 18.29 kcal/mol.

Figure 3. Secondary reaction of IM1-3 and IM1-4. Unit: kcal/mol. Δ*E*: the potential barriers; Δ*H*: reaction heats (0 K).

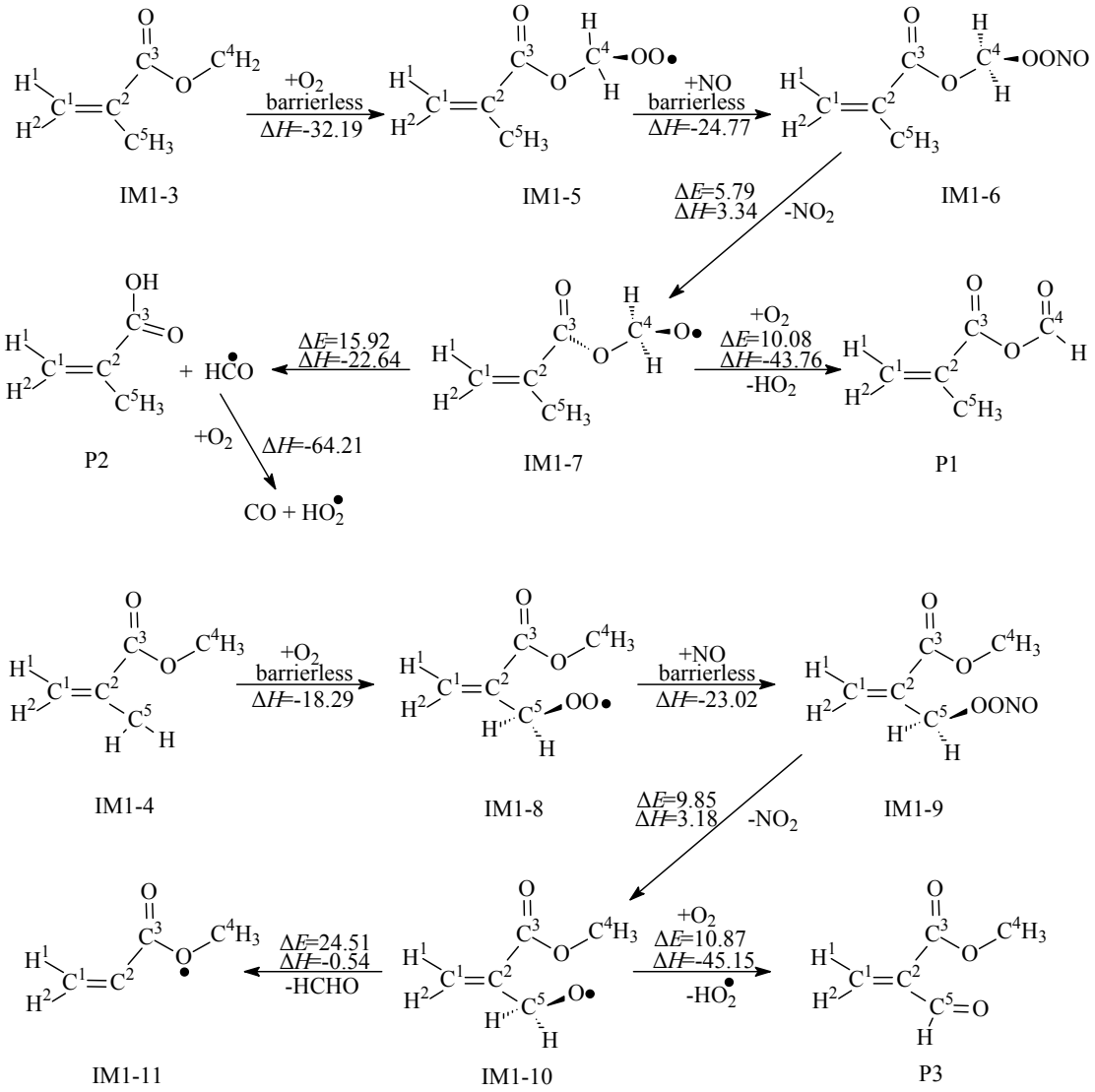

In the troposphere, IM1-5 or IM1-8 will react immediately with ubiquitous NO. The entrance channel of the reactions is exoergic, leading to two vibrationally excited intermediates (denoted as IM1-6 and IM1-9), which promptly react via unimolecular decomposition. Unimolecular decompositions of IM1-6 and IM1-9 occur via cleavage of the O-O bond, forming NO_2 and two alkoxy

radicals IM1-7 and IM1-10. The two unimolecular decomposition processes are endothermic with high potential barrier. IM1-7 can further react with O_2, followed by loss of HO_2, to form CH_2=C(CHO)$COOCH_3$ (P1) and HO_2, or via unimolecular decomposition and H migration to form CH_2=C(CH_3)C(O)OC(O)OH (P2). The decomposition of IM1-10 has a high barrier of 24.51 kcal/mol and cannot occur under the general atmospheric conditions. The reaction with O_2 is the primary removal pathway for IM1-10, and the products are CH_2=C(CHO)$COOCH_3$ (P3) and HO_2.

Figure 4. Secondary reaction of IM1a and IM1b. Unit: kcal/mol. Δ*E*: the potential barriers; Δ*H*: reaction heats (0 K).

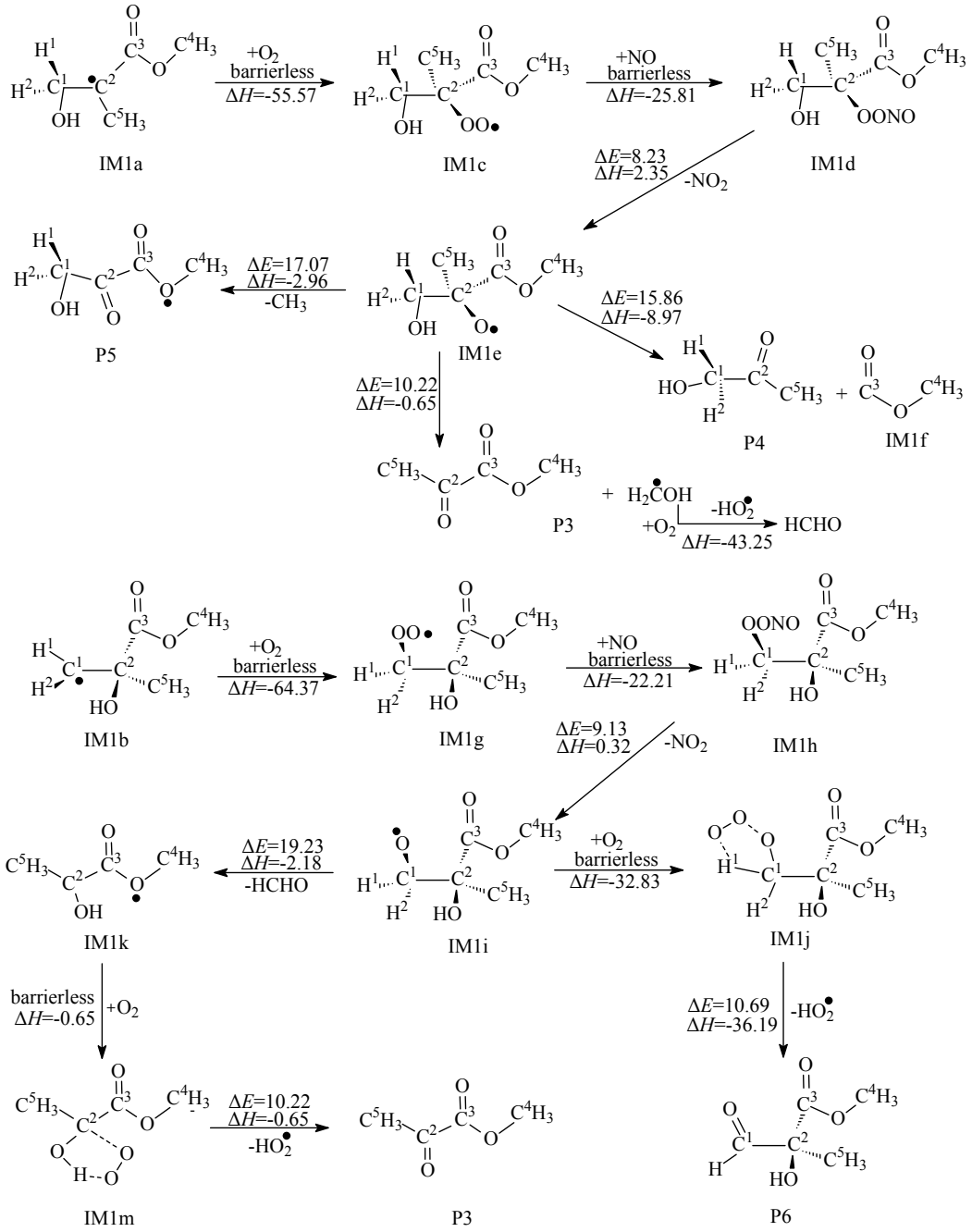

2.1.2. Addition of OH to MMA

Two carbon atoms in the C=C bond of MMA are not equivalent, thus, OH radicals can attack C^1 or C^2 atom to form two different adducts, IM1a and IM1b, as shown in Figure 1. The OH-MMA adducts, IM1a and IM1b, could easily further react with O_2/NO in the atmosphere and form intermediates IM1d and IM1h, respectively. As shown in Figure 4, the two addition steps are barrierless and strongly exothermic. Then, the energy-rich intermediates IM1d and IM1h can decompose to yield IM1e and IM1i. The two decomposition processes are endothermic with high potential barriers. Three possible unimolecular decomposition pathways from IM1e were identified. The first pathway occurs via H migration and breaking of C^2–C^5 bond to yield P3. The barrier height is 10.22 kcal/mol. The second and third decomposition pathways are cleavage of C^1–C^2 and C^2–C^3 bonds, with barriers of 17.07 and 15.86 kcal/mol. The results show that the first decomposition pathway is energetically more favorable. Unimolecular decomposition of IM1i only occurs via cleavage of C^1–C^2 bond to yield IM1k. In addition, IM1i can further react with O_2, followed by the loss of HO_2, to yield $CH_3OC(O)C(CH_3)(OH)CHO$ (P6). The decomposition of IM1i needs to overcome a barrier of 19.23 kcal/mol, therefore, the reaction with O_2 is relatively more favorable under the general atmospheric conditions. The calculated results suggest that the main products from secondary reactions of OH-MMA adducts are P3, HO_2 and methanal.

Figure 5. Decomposition and isomerization reactions of IM2a and IM2b. Unit: kcal/mol. Δ*E:* the potential barriers; Δ*H*: reaction heats (0 K).

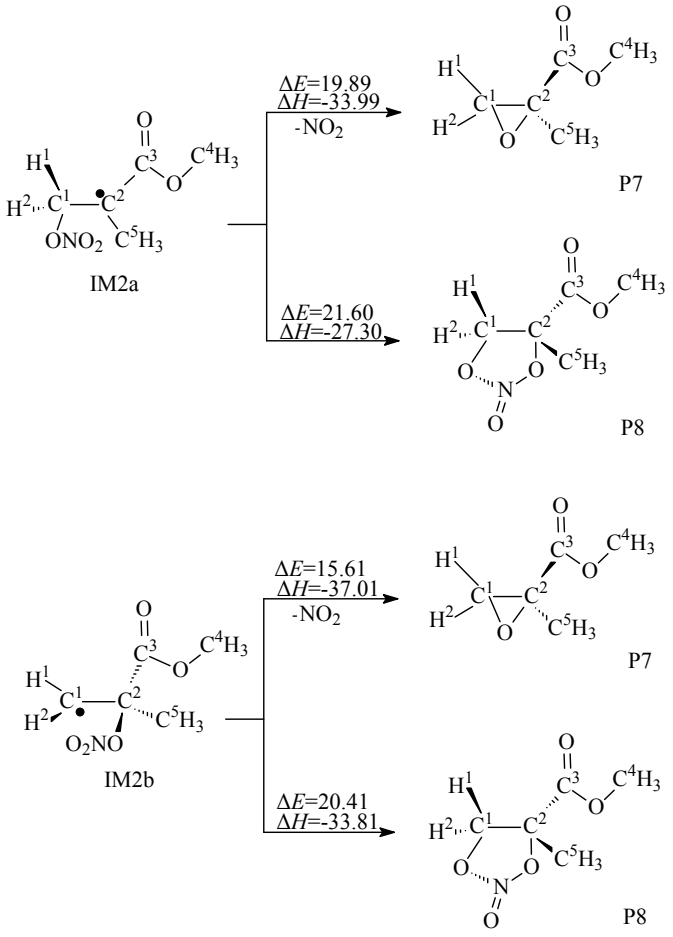

2.1.3. Addition of NO_3 to MMA

Similar to OH addition to MMA, the addition of NO_3 to MMA can form two different NO_3-MMA adducts, IM2a and IM2b, as shown in Figure 2. The scanned profile of the potential energy surface shows that the two addition reactions are barrierless. The NO_3-MMA adducts can further react via decomposition or isomerization, as depicted in Figure 5, or be removed via reactions with O_2/NO, as depicted in Figure 6. As shown in Figure 5, in the decomposition processes, a three-membered ring product, P7, was generated from the intermediates IM2a and IM2b via loss of NO_2, with potential barriers of 19.89 and 15.61 kcal/mol; and a five-membered ring product, P8, was formed from the isomerization of IM2a and IM2b, with potential barriers of 21.60 and 20.41 kcal/mol. The results suggest that the decomposition and isomerization processes are competitive.

Figure 6. Secondary reaction of IM2a and IM2b. Unit: kcal/mol. Δ*E*: the potential barriers; Δ*H*: reaction heats (0 K).

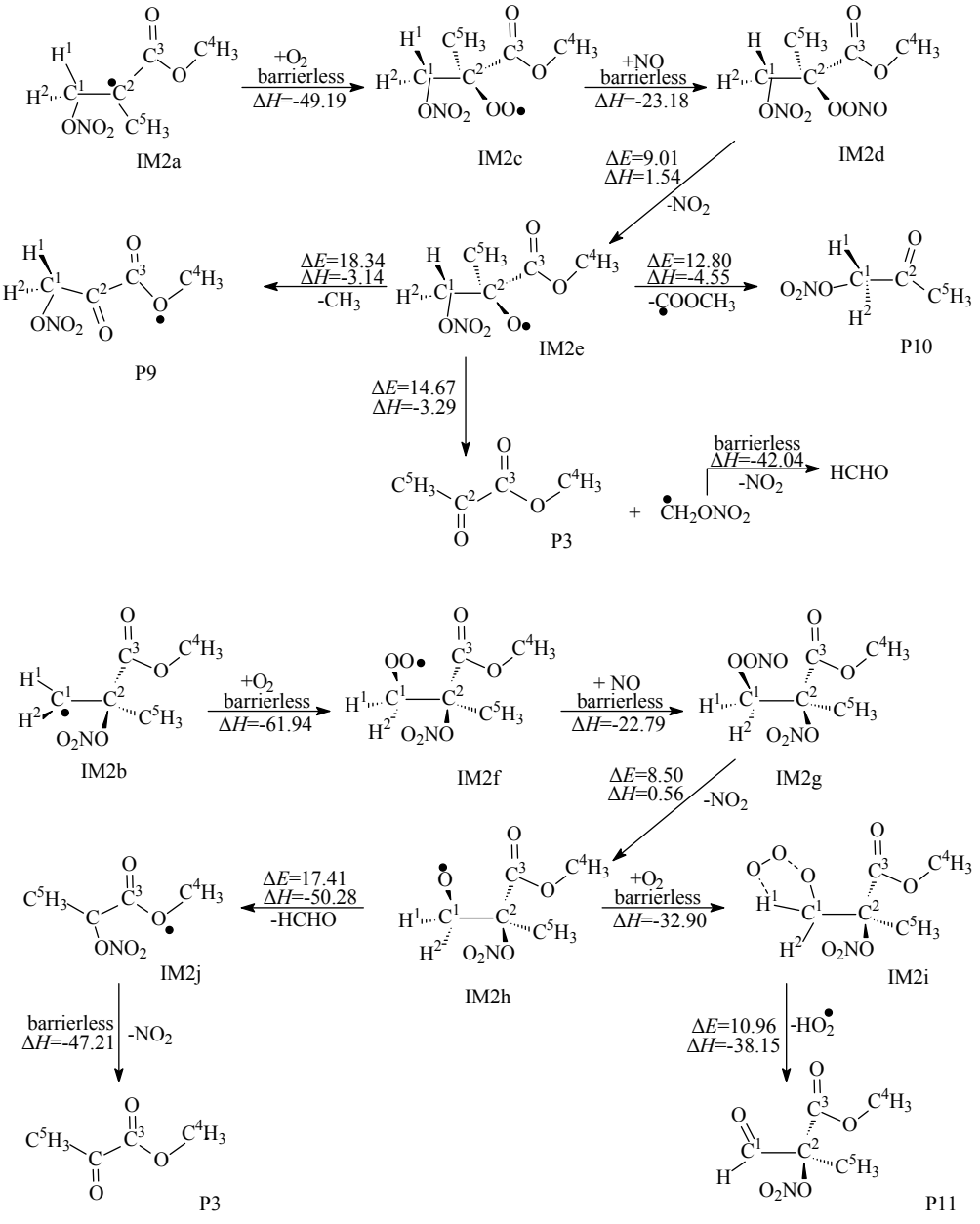

In the oxygen-rich atmosphere, the NO_3-MMA adducts could further react with O_2 to yield organic peroxy radicals. The detailed subsequent reactions are presented in Figure 6. The reactions of IM2a and IM2b with O_2 are barrierless and strongly exothermic by 49.19 and 61.94 kcal/mol to form IM2c and IM2f. In the troposphere, the two intermediates, IM2c and IM2f, will further react with ubiquitous NO immediately and yield two vibrationally excited intermediates, IM2d and IM2g, respectively. Unimolecular decompositions of IM2d and IM2g result in the formation of IM2e and IM2h via loss of NO_2. The alkoxy radical IM2e can further react via three possible unimolecular decomposition pathways, as depicted in Figure 6. Comparison of potential barriers of the three pathways shows that cleavage of the C^1–C^2 and C^2–C^3 bonds are energetically favorable, leading to the products of P3, P11 and methanal. IM2j produced from the decomposition of IM2h can further decompose to yield P3 via the loss of NO_2. This process is exothermic by 47.21 kcal/mol. IM2j can also further react with O_2, followed by the loss of HO_2 to produce P11. Calculations show that the reaction of IM2j with O_2 is energetically more favorable than the decomposition of IM2j. Comparison of the three kinds of the reaction pathways for NO_3-MMA adducts suggests that the reaction of the NO_3-MMA adduct with O_2/NO is thermodynamically and energetically more favorable than their unimolecular decomposition or isomerization.

2.2. Rate Constant Calculations

On the basis of the profile of the potential energy surface calculated by the CCSD(T)/6-31G(d) + CF//B3LYP/6-31G(d,p) method, the individual and overall rate constants for the OH and NO_3 radical-initiated reactions of MMA were calculated over the temperature range from 180 to 370 K, which is the typical temperature range of the troposphere. The rate constants of H abstraction from MMA were calculated by using the CVT/SCT method. The individual rate constants for the H abstraction pathways 1–8 are noted as k_{abs}^1–k_{abs}^8, respectively. For the addition pathways, the rate constants were calculated by using the multichannel RRKM method. The rate constants for addition of OH to the C^1 and C^2 atoms of MMA are noted as k_{OH}^1 and k_{OH}^2, respectively; and the rate constants for addition of NO_3 to the C^1 and C^2 atoms are noted as k_{NO3}^1 and k_{NO3}^2, respectively. The overall rate constant for the reaction of MMA with OH radical is noted as k_{OH}, $k_{OH} = k_{OH}^1 + k_{OH}^2 + k_{abs}^1 + k_{abs}^2 + k_{abs}^3 + k_{abs}^4$; and the overall rate constant for the reaction with NO_3 radical is noted as k_{NO3}, $k_{NO3} = k_{NO3}^1 + k_{NO3}^2 + k_{abs}^5 + k_{abs}^6 + k_{abs}^7 + k_{abs}^8$. Comparison of the rate constants of the H abstraction pathways and addition pathways shows that the H abstraction pathways can be negligible for their little contribution under the general atmospheric conditions.

At 298 K, the calculated overall rate constants for the reactions of MMA with OH and NO_3 radicals are 4.36×10^{-11} and 3.64×10^{-15} cm^3 $molecule^{-1}$ s^{-1}, excellently agreed with the available experimental values [13,18,19]. The good agreement infers that the calculated other rate constants are reasonable. The calculated overall rate constants are fitted over the temperature range of 180−370 K, and Arrhenius formulas are given in units of cm^3 $molecule^{-1}$ s^{-1}:

$$k(T)(\text{MMA} + \text{OH}) = (1.83 \times 10^{-12})\exp(945.58/T) \quad (1)$$

$$k(T)(\text{MMA} + \text{NO}_3) = (6.75 \times 10^{-16})\exp(502.48/T) \quad (2)$$

To assess the impact to the environment, it is critical to known the atmospheric lifetime of MMA. The global average concentration OH radical (c_{OH}) in daytime is 2×10^6 molecule/cm^3 [20], and the typical concentration of NO_3 radicals (c_{NO3}) in the continental boundary layer is 5×10^8 molecule/cm^3 [21]. According to the rate constants of the reactions of MMA with OH and NO_3 radicals, using the expression:

$$\tau_{OH} = \frac{1}{k_{(OH+MMA)} \times c_{OH}} \quad (3)$$

$$\tau_{NO_3} = \frac{1}{k_{(NO_3 + MMA)} \times c_{NO_3}} \quad (4)$$

The atmospheric lifetimes of MMA determined by OH and NO_3 radicals are 3 h and 6.5 days, respectively. The obtained lifetimes here can be comparable to 2–10 h for OH radicals [21] and 6 days for NO_3 radicals in the previous work [14]. Therefore, MMA is likely to be removed quickly by the reaction with OH radicals near to their emission sources. However, since the atmospheric lifetime of MMA were determined both by the rate constant of the reactions with radicals and the concentration of radicals, in some seriously polluted regions, the reaction with NO_3 radicals also may contribute to the removal of MMA in the atmosphere. Moreover, in some coastal areas where the concentration of Cl atoms can reach a peak value of 1×10^5 molecule/cm^3 [22,23], the MMA may be quikly removed by the reaction with Cl atoms [15].

3. Computational Methods

All the calculations were performed with the Gaussian 03 software package (Gaussian, Inc., Wallingford, CT, USA). Geometrical parameters of the reactants, intermediates, transition states, and products were fully optimized at the B3LYP level with a standard basis set 6-31G(d,p). The nature of stationary points, the zero-point energy (ZPE), and the thermal contribution to the free energy of activation were determined by the vibrational frequency calculation at the same level. For each transition state, the intrinsic reaction coordinate (IRC) calculation was performed using the same electronic structure theory to confirm it was connected to the right minima along the reaction pathway. The DFT geometries were then used in the single-point energy calculations at the frozen-core second-order Møller-Plesset perturbation theory (MP2) and the coupled-cluster theory with single and double excitations including perturbative corrections for the triple excitations (CCSD(T)) with several basis sets. Each single-point energy was further corrected using a factor, CF. This factor was determined from the energy difference between the MP2/6-311++G(d,p) and MP2/6-31G(d) levels, and the ranges of CF value are 0.001592 to 0.3571924 Hartree in the reactions of MMA with OH radical, and 0.010456 to 0.2470771 Hartree in the reactions of MMA with NO_3 radical. The values of calculated energies at the CCSD(T)/6-31G(d) level were then corrected by the CFs, corresponding to the CCSD(T)/6-31G(d) + CF level of theory [24,25]. Potential barriers (ΔE, $\Delta E = E_{\text{transition state}} - \Sigma E_{\text{reactants}}$) and reaction heats ($\Delta H$, $\Delta H = \Sigma E_{\text{products}} - \Sigma E_{\text{reactants}}$) were determined in each channel.

Depending on different reaction types, two methods were used to calculate the rate constants. For the abstraction pathways, the widely used canonical variational transition-state theory with the small curvature tunneling (CVT/SCT) correction was adopted. The theoretical rate constants and their

temperature dependence were calculated by using the Polyrate 9.3 program (University of Minnesota, Minneapolis, MN, USA). Actually, the CVT/SCT method has been successfully used in dealing with several bimolecular reactions [26]. For the addition pathways, the rate constants were calculated using multichannel Rice-Ramspergere-Kassele-Marcus (RRKM) theory. This method has been successfully used in the previous works for several addition reactions [27].

4. Conclusions

A theoretical study was performed on the mechanism of OH and NO_3 radical-initiated reactions of methyl methacrylate. The rate constants were calculated by using the CVT/SCT and multichannel RRKM method. Several specific conclusions can be drawn from this study:

(1). The mechanism of OH and NO_3 radical-initiated reactions of MMA includes H abstraction pathways and the addition pathways, and the H abstraction pathways can be negligible because of their little contribution under the general atmospheric conditions.

(2). The OH-MMA and NO_3-MMA adducts are open-shell activated radical intermediates, and can further react with O_2/NO in the atmosphere. For the OH radical-initiated reaction, the main products are $CH_3C(O)C(O)OCH_3$, HO_2 and methanal, consistent with the experimental results [15]. For the NO_3 radical-initiated oxidation, the reaction of the NO_3-MMA adduct with O_2/NO is thermodynamically and energetically more favorable than their unimolecular decomposition or isomerization under the general atmospheric conditions and the main products are $CH_3C(O)C(O)OCH_3$, $CH_3C(O)CH_2NO_3$ and methanal.

The calculated overall rate constants match well the available experimental values. The atmospheric life times of MMA determined by OH radicals and NO_3 radicals are 3 h and 6.5 days. NO_3-initiated oxidation reaction contributes little to the atmospheric losses of MMA except in polluted regions.

Acknowledgments

This work was supported by NSFC (National Natural Science Foundation of China, project Nos. 21337001 and 21177077), Independent Innovation Foundation of Shandong University (IIFSDU, project No. 2012JC030) and Taishan Grand (No. ts20120522). The authors thank Donald G. Truhlar for providing the POLYRATE 9.3 program.

Conflicts of Interest

The authors declare no conflict of interest.

References

1. Mayo, F.R.; Lewis, F.M. Copolymerization. I. A basis for comparing the behavior of monomers in copolymerization; the copolymerization of styrene and methyl methacrylate. *J. Am. Chem. Soc.* **1944**, *66*, 1594–1601.
2. Scott, M.P.; Brazel, C.S.; Benton, M.G.; Mays, J.W.; Holbrey, J.D.; Rogers, R.D. Application of ionic liquids as plasticizers for poly(methyl methacrylate). *Chem. Commun.* **2002**, 1370–1371.

3. Srinivasan, S.; Chhatre, S.S.; Mabry, J.M.; Cohen, R.E.; McKinley, G.H. Solution spraying of poly(methyl methacrylate) blends to fabricate microtextured, superoleophobic surfaces. *Polymer* **2011**, *52*, 3209–3218.
4. Nagai, K. New developments in the production of methyl methacrylate. *Appl. Catal. Gen.* **2001**, *221*, 367–377.
5. Brune, D.A.G.; Beltesbrekke, H. Levels of methylmethacrylate, formaldehyde, and asbestos in dental workroom air. *Eur. J. Oral Sci.* **1981**, *89*, 113–116.
6. Zhu, J.; Newhook, R.; Marro, L.; Chan, C.C. Selected volatile organic compounds in residential air in the city of ottawa, canada. *Environ. Sci. Technol.* **2005**, *39*, 3964–3971.
7. Borzelleca, J.F.; Larson, P.S.; Hennigar G.R.; Huf, E.G.; Crawford, E.M.; Smith, R.B., Jr. Studies on the chronic oral toxicity of monomeric ethyl acrylate and methyl methacrylate. *Toxicol. Appl. Pharm.* **1964**, *6*, 29–36.
8. Leggat, P.A.; Kedjarune, U. Toxicity of methyl methacrylate in dentistry. *Int. Dent. J.* **2003**, *53*, 126–131.
9. Singh, A.R.; Lawrence, W.H.; Autian, J. Embryonic-fetal toxicity and teratogenic effects of a group of methacrylate esters in rats. *J. Dent. Res.* **1972**, *51*, 1632–1638.
10. Canosa-Mas, C.E.; Carr, S.; King, M.D; Shallcross,D E; Thompson, K.C; Wayne, R.P. A kinetic study of the reactions of NO_3 with methyl vinyl ketone, methacrolein, acrolein, methyl acrylate and methyl methacrylate. *Phys. Chem. Chem. Phys.* **1999**, *1*, 4195–4202.
11. Grosjean, D.; Grosjean, E.; Williams, E.L. Rate constants for the gas-phase reactions of ozone with unsaturated alcohols, esters, and carbonyls. *Int. J. Chem. Kinet.* **1993**, *25*, 783–794.
12. Saunders, S.M.; Baulch, D.L.; Cooke, K.M.; Pilling, M.J.; Smurthwaite, P.I. Kinetics and mechanisms of the reactions of OH with some oxygenated compounds of importance in tropospheric chemistry. *Int. J. Chem. Kinet.* **1994**, *26*, 113–130.
13. Blanco, M.B.; Taccone, R.A.; Lane, S.I.; Teruel, M.A. On the OH-initiated degradation of methacrylates in the troposphere: Gas-phase kinetics and formation of pyruvates. *Chem. Phys. Lett.* **2006**, *429*, 389–394.
14. Wang, K.; Ge, M.; Wang, W. Kinetics of the gas-phase reactions of NO_3 radicals with ethyl acrylate, *N*-butyl acrylate, methyl methacrylate and ethyl methacrylate. *Atmos. Environ.* **2010**, *44*, 1847–1850.
15. Blanco, M.B.; Bejan, I.; Barnes, I.; Wiesen, P.; Teruel, M.A. Products and mechanism of the reactions of OH radicals and Cl atoms with methyl methacrylate (CH_2=C(CH_3)C(O)OCH_3) in thepresence of NOx. *Environ. Sci. Technol.* **2014**, *48*, 1692–1699.
16. Hollenstein, H.; Günthard, H.H. Solid state and gas infrared spectra and normal coordinate analysis of 5 isotopic species of acetaldehyde. *Spectrochim. Acta Mol. Biomol. Spectrosc.* **1971**, *27*, 2027–2060.
17. Kuchitsu, K.; Graner, G. *Structure of Free Polyatomic Molecules: Basic Data*; Springer Verlag: Berlin, Germany, 1998; pp. 1–25.
18. Prinn, R.G.; Huang, J.; Weiss, R.F.; Cunnold, D.M.; Fraser, P.J.; Simmonds, P.G.; McCulloch, A.; Harth, C.; Salameh, P.; O'Doherty, S.; *et al.* Evidence for substantial variations of atmospheric hydroxyl radicals in the past two decades. *Science* **2001**, *292*, 1882–1888.

19. Teruel, M.A.; Lane, S.I.; Mellouki, A.; Solignac, G.; Le Bras, G. OH reaction rate constants and Uv absorption cross-sections of unsaturated esters. *Atmos. Environ.* **2006**, *40*, 3764–3772.
20. Shu, Y.; Atkinson, R. Atmospheric lifetimes and fates of a series of sesquiterpenes. *J. Geophys. Res.* **1995**, *100*, 7275–7281.
21. Blanco, M.B.; Teruel, M.A.; Bejan, I.; Barnes, I.; Wiesen, P. Methyl methacrylate in the atmosphere: OH- and Cl-initiated oxidation in the gas phase. In *Simulation and Assessment of Chemical Processes in a Multiphase Environment*; Barnes, I., Kharytonov, M.M., Eds.; Springer Netherlands: Houten, The Netherlands, 2008; pp. 485–494.
22. Ezell, M.J.; Wang, W.; Ezell, A.A.; Soskin, G.; Finlayson-Pitts, B.J. Kinetics of reactions of chlorine atoms with a series of alkenes at 1 Atm and 298 K: Structure and reactivity. *Phys. Chem. Chem. Phys.* **2002**, *4*, 5813–5820.
23. Spicer, C.W.; Chapman, E.G.; Finlayson-Pitts, B.J.; Plastridge, R.A.; Hubbe, J.M.; Fast, J.D.; Berkowitz, C.M. Unexpectedly high concentrations of molecular chlorine in coastal air. *Nature* **1998**, *394*, 353–356.
24. Lei, W.; Zhang, R. Theoretical study of hydroxyisoprene alkoxy radicals and their decomposition pathways. *J. Phys. Chem. A* **2001**, *105*, 3808–3815.
25. McGivern, W.S.; Suh, I.; Clinkenbeard, A.D.; Zhang, R.; North, S.W. Experimental and computational study of the OH-isoprene reaction: Isomeric branching and low-pressure behavior. *J. Phys. Chem. A* **2000**, *104*, 6609–6616.
26. Hou, H.; Wang, B. Ab initio study of the reaction of propionyl (C_2H_5CO) radical with oxygen (O_2). *J. Chem. Phys.* **2007**, *127*, 1–9.
27. He, M.; Cao, H.; Sun, Y.; Han, D.; Hu, J. Mechanistic and kinetic study of the gas-phase reaction of vinyl acetate with ozone. *Atmos. Environ.* **2012**, *49*, 197–205.